Equilibrium morphologies for Cl-roughened Si(100) at 700–750 K: Dependence on Cl concentration

G. J. Xu, Koji S. Nakayama, B. R. Trenhaile, C. M. Aldao,* and J. H. Weaver

Department of Materials Science and Engineering, Department of Physics, and Frederick Seitz Materials Research Laboratory,

University of Illinois at Urbana-Champaign, Urbana, Illinois 61801

(Received 15 November 2002; published 31 March 2003)

Adsorbed halogen atoms on Si(100)- (2×1) can induce roughening at temperatures where material removal (etching) is minimal. Variable temperature scanning tunneling microscopy was used to follow roughening at 700-750 K for surfaces with 0.1-0.99 ML of Cl. Dimer vacancies and Si adatoms were observed at short times, and at longer times the progression toward a state of dynamic equilibrium was traced. Once dynamic equilibrium was reached, the appearance of individual pits and regrowth islands changed but their densities and mean sizes did not. The results show that the roughness depends nonlinearly on Cl coverage with surfaces having 0.3 ML being nearly ten times rougher than those with 0.1 ML. The importance of Cl-free dimers is stressed, and the role of Cl as an impediment for vacancy and adatom diffusion is demonstrated. Roughening is attributed mainly to adsorbate-adsorbate repulsive interactions.

DOI: 10.1103/PhysRevB.67.125321 PACS number(s): 68.37.Ef, 61.43.Bn, 68.35.Ja

I. INTRODUCTION

A number of recent studies have used scanning tunneling microscopy (STM) to observe atomic-scale structural changes that accompany spontaneous etching of Si by halogens.^{1–8} These visualizations of post-etch morphologies have led to a deeper understanding of the various reaction pathways of etching. Inherit in etching is Si dihalide desorption and surface defect formation. However, a recent study⁹ demonstrated that roughening could be induced by Cl and Br at temperatures where desorption was minimal, i.e., roughening without etching. This roughening pathway was deduced from STM images obtained at room temperature after processing at 775 K. What is not known about roughening is the equilibrium morphologies different halogens and halogen concentrations, the way in which the surface evolves to equilibrium, and the underlying mechanisms that cause the system to roughen.

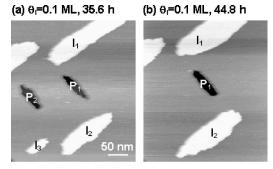
In this paper, we focus on the time evolution and the equilibrium morphologies for Cl-Si(100)-(2 \times 1), with special attention to the dependence on Cl concentration at 700 K. Using a variable temperature scanning tunneling microscope (VT-STM), we have imaged samples for extended periods of time. At 700 K, roughening is the dominant process as single-layer pits and regrowth features form without Si removal. Healing also occurs when dimer vacancies (DVs) and mobile Si atoms are accommodated at steps. Once dynamic equilibrium is reached, the densities and mean sizes of surface features remain unchanged though individual features continue to fluctuate in size and shape. The halogen concentration, which remains nearly constant, dictates the diffusivities of the Si and Cl adatoms and the DVs. It also controls the reaction rate since roughening can only occur when there are halogen-free dimers adjacent to the reaction site. 9,10 At low and intermediate coverages, the reaction rate is high and, while the mobilities are too high to follow individual events, the evolution of pits and islands can be followed. We show

that surfaces become rougher with increasing Cl concentration as the pit and regrowth island sizes diminish but their densities increase. For nearly saturated surfaces, the roughening reaction is slow, the Si and DV mobility is strongly hindered, and the system does not reach equilibrium over our time scale of $\sim\!20\,$ h.

II. EXPERIMENT

The experiments were performed in an ultrahigh vacuum system (base pressure of $<4\times10^{-11}$ Torr) using an Omicron VT-STM. The p-type Si wafers were B doped and had a resistivity of $0.01-0.012~\Omega$ cm. They were oriented within 0.5° of (100). Typical Si(100)-(2×1) surfaces had an initial surface defect concentration of 0.01-0.02~ML. Cleaning was done by degassing at 875 K for $\sim12~\text{h}$ and heating to 1475 K for 90 sec. The temperature was monitored with an optical pyrometer during sample preparation. During scanning, it was adjusted by varying the heating power (reproducibility $\pm10~\text{K}$).

The halogen source was a solid-state electrochemical cell based on a AgCl pellet that was doped with $\sim 5\%$ CdCl₂. An applied electric field attracted Cl ions to a Pt mesh where they combined and desorbed as Cl2. The current through the cell was 5 μ A, giving a flux of 1.6×10^{13} molecules per second. Samples were exposed for varying amounts of time to achieve the desired Cl coverage. 11 The coverage was determined directly from STM images since dimers with Cl can be distinguished from bare dimers when scanning with -1.3 V sample bias at room temperature. Samples were heated to 700 K after the initial coverages were established. Filled-state images were acquired with Pt/Ir tips in a constant current mode. Scans took 7–35 min, depending on the image resolution and the scan speed. Sequential images were acquired by scanning from left to right, bottom to top in the images shown in the figures, and the time identified corresponds to the start time of each scan.



(c) θ_i=0.1 ML, 4.6 h

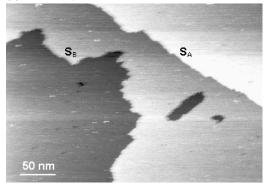


FIG. 1. STM images (a) and (b) represent the equilibrium morphology for 0.1 ML Cl on Si(100) at 700 K. While the average feature size, surface area, and density did not change, the details in a given region were still dynamic. Large features such as islands I_1 and I_2 and pit P_1 changed shape and size over the course of ~ 9 h. I_3 and P_2 disappeared as a consequence of attachment and detachment fluctuations. While the appearance of the S_A in (c) has a relatively low kink density, such as for clean Si(100), roughening with Cl results in large peninsulas and gulfs at the intrinsically rougher S_B steps. Likewise S_A steps for the RI and pit features are much more regular than the S_B steps of those features.

III. RESULTS AND DISCUSSION

The roughening pathway for Si(100) was discovered by Nakayama et al. They reported that thermally activated roughening involved Cl-induced reactions in which DVs and Si regrowth islands (RIs) can be produced without desorption, i.e., without etching. They proposed a sequence of events in which a Si dimer with two Cl adatoms undergoes an isomerization reaction, forming SiCl2 and a Si atom with two dangling bonds. The Si atom is thereby destabilized and it can escape onto the terrace. The SiCl₂ species cannot decay via the reverse isomerization pathway since one of the Si atoms has been replaced by a vacancy. At high temperature, SiCl₂ can desorb in a process termed vacancy-assisted desorption or etching. 12-15 At temperatures for which desorption is not likely, the SiCl₂ unit can decay by transferring the Cl atoms to nearby Cl-free sites. If this happens, the nowbare Si atom can also escape onto the terrace. The result is a DV and two Si adatoms that can form regrowth structures. The Cl atoms can then participate in subsequent reactions. Competing with roughening are healing processes whereby mobile DVs and adatoms are accommodated at steps, including those associated with extended pits and islands.

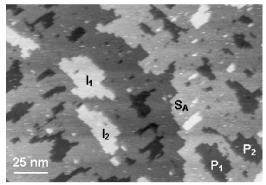
A key element in the roughening (and etching) pathway is that halogen-free dimers must exist adjacent to the reaction site—they are the sites to which Si must escape. Figures 1–4 show the consequence of roughening as a function of Cl concentration under conditions where there is minimal Cl loss (confirmed by imaging at ambient temperature). At low and intermediate coverage, the surface evolves quickly but at high coverage, Fig. 4, the requisite bare sites are too few and both reaction and diffusion are suppressed. As discussed below, Figs. 1–3 represent dynamic equilibrium morphologies where the details of a particular feature fluctuate, as revealed by the images, but the size distributions and densities for pits and RIs do not change. The morphology of Fig. 4 reflects transient reaction and roughening.

The images in Figs. 1(a) and 1(b) were acquired \sim 35.6 h and ~44.8 h after the sample reached 700 K. The initial coverage was $\theta_i(Cl) = 0.1$ ML. Early images showed transient processes related to Ostwald ripening of both pits and RIs as DVs and Si atoms were exchanged and larger features grew at the expense of smaller ones. Dynamic equilibrium was reached after ~ 2 h. The average pit size was then \sim 621 nm² and the average RI size was \sim 532 nm². Pits covered $\sim 5.8\%$ of the surface area and RIs covered $\sim 5.3\%$. The densities of pits and RIs were $\sim 100 \ \mu \text{m}^{-2}$ each. Though these values did not change, the details in a given image were still very dynamic. Island I_1 in Fig. 1(a), for example, altered its shape to a lower aspect ratio after an elapsed time of ~ 9.2 h. Over the same period, I_2 and P_1 changed shape and increased in size by ~ 8300 and ~ 1500 dimers, respectively. Some features also disappeared as a consequence of fluctuations in size and shape. For example, I_3 and P_2 , which were derived from ~ 1700 and ~ 3400 dimers, fluctuated and finally disappeared after ~ 70 min and \sim 8.8 h, respectively.

Figure 1(c) makes it possible to visualize changes in the step profile. For clean surfaces, S_A steps (which run parallel to the dimer rows) have a low kink density while S_B steps (perpendicular to dimer rows) are much less regular because the energy to form a kink on an S_B step is much lower than that on an S_A step. Step motion occurs through the exchange of atoms with the reservoir of Si adatoms on the terraces, and the pattern in equilibrium reflects the interaction energies between dimers. 16,17 The limited roughness of clean Si steps makes it possible to analyze them in terms of kinks assuming no overhangs. Here, we see that Cl has a profound effect and, although overhangs are not dominant, large peninsulas and gulfs characterize the S_B steps, Fig. 1(c). This is remarkable since it implies that Cl in small concentrations can alter the effective substrate dimer-dimer interactions. Conversely, S_A steps are not significantly altered at this coverage and they show a similar roughness to those of clean Si(100).

Images for 0.3 ML Cl-Si(100) showed that it took longer to reach equilibrium compared to 0.1 ML. Sequential scans showed small islands and pits that grew, shrank, and disappeared as new ones were created. By \sim 4 h, the surface had reached dynamic equilibrium and the images of Fig. 2 are representative of this configuration with rapidly changing local morphologies. Islands I_1 and I_2 and several surrounding pits show significant changes as they captured and released

(a) θ_1 =0.3 ML, 10.7 h



(b) θ_i =0.3 ML, 10.9 h

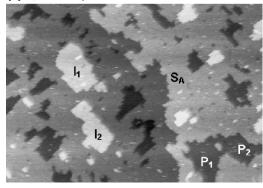
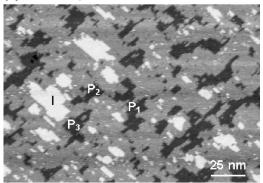


FIG. 2. (a) and (b) represent the equilibrium morphology for 0.3 ML Cl-Si(100) at 700 K. Islands I_1 and I_2 and several surrounding pits changed as they captured and released Si adatoms and DVs. Pits P_1 and P_2 merged and a remnant island was cut off from the main terrace. The pits and RIs of Fig. 2 are a factor-of-10 smaller than those of Fig. 1 (note the scale difference). Pits and RI features also occupied \sim 2.5 times more space on the terrace for 0.3 ML than for 0.1 ML. Roughening of S_A steps is now evident with deep gulfs and overhangs.

Si adatoms and DVs. Figure 2(b) shows that pits P_1 and P_2 merged and a small residual island was isolated in the center of the merged area. Compared to Fig. 1, the pits and RIs were a factor-of-10 smaller (average pit size ~ 54 nm², average RI size ~ 52 nm²). I_2 in Fig. 1(b) is ~ 13 times the size of I_2 in Fig. 2(b) and P_1 in Fig. 1(b) is ~ 1.5 times the combined size of P_1 and P_2 in Fig. 2(b) (note the difference in scales). Moreover, both the pits and RIs covered $\sim 14\%$ of the surface area; they occupied ~ 2.5 times more space on the terrace for 0.3 ML than for 0.1 ML. The densities of pits and RIs were $\sim 2600~\mu\text{m}^{-2}$ each. S_A steps, such as those shown, were rough and had rapidly evolving patterns. In contrast to the S_A step in Fig. 1(c), steep gulfs and overhangs were apparent in the step of Fig. 2.

Figure 3 shows a surface for which $\theta_i(\text{Cl})$ was 0.5 ML (same scale as Fig. 2). Dynamic equilibrium was reached after ~ 8 h. As shown, the appearance of the small RIs around island I in Fig. 3(a) changed substantially in 0.2 h. Likewise, pits $P_1 - P_3$ all showed changes, and many small features appeared or disappeared across the surface. Here, the pits and RIs had average sizes of ~ 38 and ~ 12 nm² and the surface was covered $\sim 18\%$ by pits and $\sim 7\%$ by RIs.

(a) θ_1 =0.5 ML, 12.0 h



(b) θ_i =0.5 ML, 12.2 h

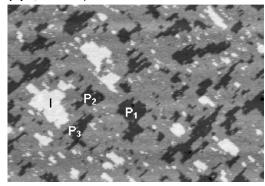


FIG. 3. (a) and (b) represent the equilibrium morphology for 0.5 ML Cl-Si(100) at 700 K (same scale as Fig. 2). Small RIs around island I in (a) changed substantially in 0.2 h (b). Over the same period, pits P1-P3 showed significant restructuring, and many small features appeared or disappeared across the surface. These pits and RIs were even smaller than those for $\theta_i(\text{Cl}) = 0.3 \text{ ML}$.

These pits and RIs were even smaller than those for $\theta_i(\text{Cl}) = 0.3$ ML. The densities of pits and RIs were ~ 4700 and $\sim 5800~\mu\text{m}^{-2}$ each. For each of these coverages, 0.1, 0.3, and 0.5 ML, the pit density and the RI density were close to each other, and they increased with coverage.

The difference between pit and RI surface area was minimal for 0.1 and 0.3 ML Cl, but the difference was significant at 0.5 ML with \sim 18% pit and \sim 7% RI surface coverage. This can be attributed to the smaller feature size and the corresponding greater average step curvature. Convex steps involve a higher average number of broken bonds per atom than do concave steps. From an energetic point of view, pits would be favored over RIs since the surface would favor concave steps (corresponding to the perimeter of pits inside the terrace) over convex steps (corresponding to the perimeter of RIs on the terrace). This effect is minimal when the feature size is large enough and the curvature is small. Although there is tenfold decrease in average feature size from 0.1 to 0.3 ML coverage, the curvature is still too low to play a significant role. With the increase of curvature, the energy difference per atom at the perimeters of pit and RI will be more profound, and this accounts for the difference between the pit and RI surface area. Note that Si atoms from unstable RIs can be accommodated at step edges.

Figure 4 shows an image taken 20.2 h after the sample

θ₁=0.99 ML, 20.2 h

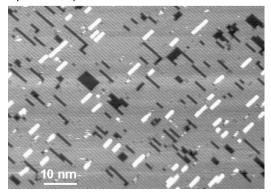


FIG. 4. STM image for a surface with a high concentration of Cl where surface reactions were sluggish (too few Cl-free dimers) and the morphology evolved slowly (frustrated diffusion). This is not the equilibrium morphology since changes in the average sizes for pits and RIs, as well as their surface area, continued to occur. Evident are small pits that were confined to a single dimer row as well as others that had branched and were wider.

reached 700 K [θ_i (Cl) on the terrace was 0.99 ML and the terrace concentration decreased to θ_f (Cl)=0.93 ML]. In this case, the high concentration of Cl inhibited surface reactions (too few Cl-free dimers) and the evolution of the surface was sluggish. Over time, however, more Cl-free dimers became available as new sites on the roughened surface accommodated Cl and limited desorption occurred. This led to an increased rate of roughening. At 20.2 h, Fig. 4, small pits had branched and some were wider than one dimer row. The RIs reached an average length of \sim 7.4 dimer units. The pits and RIs had average sizes of \sim 3.5 and \sim 2.3 nm², and the surface was covered \sim 8% by pits and \sim 4% by RIs. This surface is far from equilibrium in that subsequent scans showed

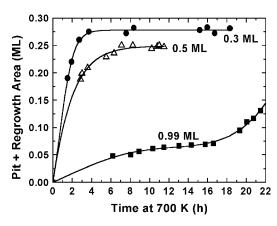


FIG. 5. The sum of pit and RI areas plotted as a function of time at 700 K. For $\theta_i(\text{Cl}) = 0.3$ and 0.5 ML, the area increased quickly but then stabilized as the surfaced reached dynamic equilibrium. It took longer for 0.5 ML since the areal density of free dimers was lower and DV and adatom diffusion was hindered by Cl. For $\theta_i(\text{Cl}) = 0.99$ ML, the surface was still evolving; the apparent increase in the roughening rate after an extended time reflects the gradual reduction in Cl concentration on the terraces (increase in alternate bonding sites).

changes in average sizes for pits and RIs, as well as their surface areas. 10

Figure 5 shows the combined pit and RI areas as a function of time at 700 K for Cl-terminated Si(100) surfaces. For $\theta_i(Cl) = 0.3$ and 0.5 ML, the combined area first increased quickly but it saturated after ~ 4 and ~ 8 h, respectively, as the surfaces reached dynamic equilibrium. Results for $\theta_i(Cl) = 0.1$ ML are not included because the roughening process was completed before high quality images could be taken (typically 1-2 h to minimize thermal drift). It a took longer time for a surface with higher Cl coverage to reach dynamic equilibrium. The effect of increased Cl concentration is to increase the density of sites where isomerization reactions can occur but also to reduce the density of bare dimers needed for recycling reactions and diffusion. The equilibrium surface roughness is also higher for higher coverage (discussed below) and many more reaction events are required to reach equilibrium. For $\theta_i(Cl) = 0.99$ ML, the surface was still in the transition stage since roughening is sluggish at high concentration.

For roughened surfaces in equilibrium, Figs. 1–3, the increase in surface energy compared to a clean surface, where the roughness is negligible, can be related to the number of broken bonds. To quantify the density of broken bonds, we determine the surface roughness by measuring the total length of the perimeters of the pits and RIs (in nm) and normalized it to the surface area (in nm²), with care taken to avoid regions where there were intrinsic steps. ¹⁸ The resulting surface roughness (in nm/nm²) is summarized in Fig. 6. It is 7.3 and 14.4 times greater for 0.3 and 0.5 ML, respectively, than for 0.1 ML. The roughness for $\theta_i(Cl) = 0.99$ ML is not included since the system is not in equilibrium. The low number of defects for clean Si(100) is a consequence of the high bonding energies among Si atoms. Cl atoms weaken the Si-Si bond strengths and the surface

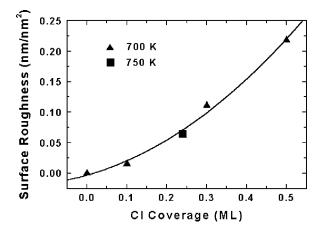


FIG. 6. Surface roughness, defined as the total length of the perimeters of the pits and RIs (in nm) over the surface area (in nm²), for Cl-Si(100) as a function of coverage. The roughness increases nonlinearly with Cl coverage because correlations in particle arrangements are important. Also included is a point for a sample that had been heated at 750 K for 3 h, where desorption (etching) was important (image shown in Fig. 7). It fits well with the trend established at 700 K since the roughness is dictated by the fast kinetic process, not the slow ones related to desorption.

(a) θ_i =0.5 ML, θ_f =0.24 ML, 3 h, 750 K

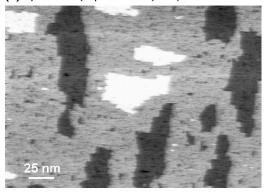


FIG. 7. STM image for a sample had been heated at 750 K for 3 h. Images acquired at ambient temperature showed that the initial and final terrace concentrations were 0.5 and 0.24 ML. Surface features similar to those of Fig. 2 are evident where the latter features were for a surface that was roughened at a constant concentration of 0.3 ML at 700 K.

roughens. A linear dependence of roughness on Cl coverage might be expected from mean-field-type considerations that do not take into account correlations in the arrangement of particles. However, Fig. 6 shows very nonlinear behavior, and this indicates that correlations in particle arrangements are important. We note that Zhdanov and Kasemo¹⁹ studied the effect of adsorption on roughening using Monte Carlo simulations that included correlations. They reported that the roughening temperature did not depend linearly on the adsorbate coverage.

The above results were obtained at 700 K where desorption was negligible. It is important to determine how the roughness would depend on concentration in a temperature regime when desorption is possible. To do this, we heated a sample with $\theta_i(C1) = 0.5 \text{ ML}$ to 750 K for 3 h and then quenched it to ambient temperature. Images such as that of Fig. 7 gave a final terrace concentration of $\theta_f(Cl)$ \sim 0.24 ML. Figure 2 shows similar features for a sample that was roughened at a constant concentration of 0.3 ML at 700 K. Analysis indicated a roughness of 0.0624 nm/nm², a value that fit well with the trend established at lower temperature, Fig. 6. While the increase in temperature accelerated surface processes, the final patterns were determined by the relative rates of those processes, and they were not significantly altered. In all cases, desorption is slow compared to the roughening and healing processes. The surface roughness is that of the equilibrium surface corresponding to the final Cl coverage, despite Cl loss and etching.

The results presented here demonstrate that adsorbed Cl plays multiple roles. First, it is the agent that causes roughening, and the extent of roughening increases with coverage. Second, Cl alters the diffusivities of Si adatoms and DVs, and it determines the rate at which the surface approaches dynamic equilibrium. An aspect of this equilibrium state is that the mobile species seek to form energetically favorable configurations, with partial healing of damage by DV annihilation or Si adatom accommodation at steps. As a result,

the surface roughness is 14.4 times greater for 0.5 ML than for 0.1 ML.

What remains uncertain is the nature of the interactions that drive the Cl-Si(100) surface to a roughened state. Based on restricted-solid-on-solid model calculations, Zhdanov and Kasemo¹⁹ proposed three general types of interactions in roughening, namely, (i) indirect next-nearest-neighbor adsorbate-substrate repulsion, (ii) attractive nearest-neighbor adsorbate-substrate lateral interaction, and (iii) repulsive adsorbate-adsorbate lateral interaction. Mechanism (i) implies that Cl would be prone to adsorb on Si ad-dimers or at the top of a step edge. Under mechanism (ii), Cl would prefer sites near step edges on the lower terrace. From STM images, however, neither one of these tendencies was detected. Moreover, Selloni and co-workers 12,20 found equal stabilities for Cl atoms adsorbed on a pristine terrace and on a dimer next to a DV on the same row, indicating that mechanism (ii) is not dominant.

There is substantial evidence that points to the importance of (iii), repulsive adsorbate-adsorbate lateral interactions. Several years ago, Rioux et al.²¹ showed the chemisorption consequence of steric repulsions for I on Si(100), namely, a $c(4\times2)$ configuration at 0.5 ML coverage. Local $c(4\times2)$ regions were also observed for Cl- or Br-terminated Si(100).^{7,15} Here, we have observed that it is rare that Cl adatoms are adjacent to each other within the same dimer row at ambient temperature, though alignment across rows is more common. These results are consistent with inter-row and intra-row steric repulsive interactions of 26 and 61 meV, respectively, proposed by Herrmann et al. based on densityfunctional calculations. ²² These repulsive interactions would make S_A steps energetically unstable for a saturated surface. Moreover, steric repulsions, involving Br and I, produced (3) ×2) domains in which dimer rows were separated by missing atom rows after surfaces were saturated and etched. 3,21 Finally, de Wiis and Selloni calculated that the (3×2) reconstructed surface is the most stable for Br-Si(100).²³

Though steric repulsion is important at high and intermediate coverages, one might expect much less impact at low coverages of 0.1 and 0.3 ML. In particular, the halogens could be adsorbed in such a way as to reduce adsorbate-adsorbate interactions. However, steric repulsive interactions of 26 and 61 meV cannot prevent Cl pairs from adsorbing at neighboring dimers at 700 K as the Boltzmann factors, $\exp(-E/kT)$, are only \sim 0.65 and \sim 0.36, respectively. These pairs can then meet and cause local pitting. Some pits can be healed by Si adatom capture. Others will diffuse via DV events and form larger features. Thus, steric repulsive interactions are likely to be the key for roughening, even at low coverage. Preliminary results of Monte Carlo modeling indicate that adsorbate-adsorbate interactions are dominant up to 0.5 ML.²⁴

IV. CONCLUSIONS

This paper has focused on the roughening of Si(100)- (2×1) under different Cl coverages at a temperature at which desorption was small, with additional insight obtained where etching was important at 750 K. We demonstrated that

the Si(100) surface roughens for any Cl coverage in differing degrees, and that the roughening pathway requires bare dimers. Moreover, the equilibrium morphologies are sensitive to Cl concentration, with roughness increasing nonlinearly with coverage θ . These results are important because they identify the role of Cl as the driving force for roughening, via adsorbate-adsorbate repulsion. They also show that it is a key component in the approach toward equilibrium, since site blocking hinders the reaction pathway and subsequent diffusion. Both roles must be considered in determining the final surface morphology.

ACKNOWLEDGMENTS

This work was supported in part by the National Science Foundation and in part by the U. S. Department of Energy, Division of Materials Sciences under Award No.DEFG02-91ER45439 through the Frederick Seitz Materials Research Laboratory at the University of Illinois at Urbana-Champaign. We thank V. Petrova, S. Burdin, and E. Sammann of the Center for Microanalysis of Materials for their expert assistance.

^{*}Permanent address: Institute of Materials Science and Technology (INTEMA), Universidad Nacional de Mar del Plata-CONICET, Juan B. Justo 4302, 7600 Mar del Plata, Argentina.

¹ J. J. Boland and J. H. Weaver, Phys. Today **51**, 34 (1998).

²C. M. Aldao and J. H. Weaver, Prog. Surf. Sci. **68**, 189 (2001).

³M. Chander, Y. Z. Li, D. Rioux, and J. H. Weaver, Phys. Rev. Lett. **71**, 4154 (1993).

⁴D. Rioux, M. Chander, Y. Z. Li, and J. H. Weaver, Phys. Rev. B 49, 11 071 (1994).

⁵D. Rioux, R. J. Pechman, M. Chander, and J. H. Weaver, Phys. Rev. B **50**, 4430 (1994).

⁶ M. Chander, D. A. Goetsch, C. M. Aldao, and J. H. Weaver, Phys. Rev. Lett. **74**, 2014 (1995).

⁷C. F. Herrmann and J. J. Boland, Surf. Sci. **460**, 223 (2000).

⁸I. Lyubinetsky, Z. Dohnálek, W. J. Choyke, and J. Y. Yates, Jr., Phys. Rev. B 58, 7950 (1998).

⁹ K. S. Nakayama, E. Graugnard, and J. H. Weaver, Phys. Rev. Lett. 88, 125508 (2002).

¹⁰G. J. Xu, E. Graugnard, V. Petrova, K. S. Nakayama, and J. H. Weaver, preceding paper, Phys. Rev. B 67, 125320 (2003).

 $^{^{11}}$ For example, the Cl coverage was $\sim\!0.5$ ML after a 600-s exposure.

¹²G. A. de Wijs, A. De Vita, and A. Selloni, Phys. Rev. Lett. **78**, 4877 (1997).

¹³G. A. de Wijs, A. De Vita, and A. Selloni, Phys. Rev. B 57, 10 021 (1998).

¹⁴K. Nakayama, C. M. Aldao, and J. H. Weaver, Phys. Rev. Lett. 82, 568 (1999).

¹⁵ K. Nakayama, C. M. Aldao, and J. H. Weaver, Phys. Rev. B 59, 15 893 (1999).

¹⁶ F. J. Williams, J. R. Sánchez, and C. M. Aldao, Surf. Sci. **391**, 260 (1997)

¹⁷H. J. Zandvliet, Rev. Mod. Phys. **72**, 593 (2000).

¹⁸W. K. Burton, N. Cabrera, and F. C. Frank, Philos. Trans. R. Soc. London, Ser. A **243**, 299 (1951).

¹⁹ V. P. Zhdanov and B. Kasemo, Phys. Rev. B 56, R10 067 (1997).

²⁰A. Selloni (private communication).

²¹D. Rioux, F. Stepniak, R. J. Pechman, and J. H. Weaver, Phys. Rev. B **51**, 10 981 (1995).

²²C. F. Herrmann, D. Chen, and J. J. Boland, Phys. Rev. Lett. 89, 096102 (2002).

²³G. A. de Wijs and A. Selloni, Phys. Rev. B **64**, 041402(R) (2001).

²⁴C. M. Aldao, S. E. Guidoni, G. J. Xu, K. S. Nakayama, and J. H. Weaver (unpublished).